Available online at www.sciencedirect.com
SCIENCE DIRECT®
Journal of Magnetic Resonance 175 (2005) 275–284
JMR Journal of Magnetic Resonance
www.elsevier.com/locate/jmr

Planar microresonators for EPR experiments

R. Narkowicz [a,c,*], D. Suter [a], R. Stonies [b]

[a] Department of Physics, University of Dortmund, Otto-Hahn-Str. 4, D-44227 Dortmund, Germany
[b] High Frequency Institute, University of Dortmund, Friedrich-Woehler-Weg 4, D-44227 Dortmund, Germany
[c] Semiconductor Physics Institute, A. Gostauto 11, LT-2600 Vilnius, Lithuania

Received 17 February 2005; revised 21 April 2005
Available online 6 June 2005

Abstract

EPR resonators on the basis of standing-wave cavities are optimised for large samples. For small samples it is possible to design different resonators that have much better power handling properties and higher sensitivity. Other parameters being equal, the sensitivity of the resonator can be increased by minimising its size and thus increasing the filling factor. Like in NMR, it is possible to use lumped elements; coils can confine the microwave field to volumes that are much smaller than the wavelength. We discuss the design and evaluation of EPR resonators on the basis of planar microcoils. Our test resonators, which operate at a frequency of 14 GHz, have excellent microwave efficiency factors, achieving 24 ns $\pi/2$ EPR pulses with an input power of 17 mW. The sensitivity tests with DPPH samples resulted in the sensitivity value 2.3×10^9 spins $\cdot$ $G^{-1}Hz^{-1/2}$ at 300 K.

Keywords: Small-volume EPR; Planar microresonators; Signal-to-noise ratio; Sensitivity; Microwave efficiency factor

1. Introduction

The conventional resonators for electron paramagnetic resonance (EPR) experiments are optimised for relatively large samples (more than 1 mm^3). As a result, the sensitivity is less than optimal for small samples [1], thin layers and interfaces [2]. Related experiments like scanning EPR and FMR (ferromagnetic resonance) microwave microscopy [3,4] also require increased spin sensitivity. Sensitivity at the level of 10^{11} spins, as it is typically achievable by the classical inductive detection method [5] is then not sufficient. Recently introduced alternative detection methods such as magnetic resonance force microscopy [6,7], scanning tunnelling microscopy [8,9], or optically detected magnetic resonance [10,11], which have already achieved or can achieve single spin sensitivity, are only applicable to specific systems and require specific operating conditions, such as low temperature and high vacuum. As a result, they do not represent a universal alternative to the inductive detection method.

Several approaches have been proposed to improve the inductive detection sensitivity. Since the sensitivity of a detector with linear response is proportional to the quality factor Q and the filling factor of the cavity η, it can be optimised by increasing one or both of these factors. For pulsed EPR experiments short ring down time is desirable. It can only be achieved at moderate Q values, which limits the possible sensitivity gain for time-resolved experiments.

The filling factor of the resonator at given frequency can be increased by dielectric loading of the cavity. The resonator volume can be reduced by inserting low-loss microwave ceramics with dielectric constants $\varepsilon \sim 30$ [12,13] as well as low-loss ferroelectric materials with ε up to 300 [14]. The resulting reduction of the resonator volume is roughly proportional to the inverse square root of the average dielectric constant ($1/\varepsilon^{1/2}$). The

* Corresponding author. Fax: +49 231 755 3516.
E-mail address: rysard.narkovic@uni-dortmund.de (R. Narkowicz).

1090-7807/$ - see front matter © 2005 Elsevier Inc. All rights reserved.
doi:10.1016/j.jmr.2005.04.014

limited value of ε restricts the possibility of increasing the filling factor this way. This essentially applies to the microstripline [2] and stripline [15,16] or folded stripline [17,18] resonator construction as well.

Another approach is to use undersized noncavity structures with dimensions less than the wavelength, such as loop-gap resonators [19–22], or solenoidal microcoils [1,23]. These lumped circuit resonators are known for concentrating the magnetic field at the sample space and for having high filling factors, but are quite difficult to manufacture in small size. Therefore if scaling down to the micrometer size is desired, planar coils represent the valid alternative. Using standard optical lithography techniques structures with dimensions of the order of a micrometer can be defined. Once defined and tested, the planar structure can be easily reproduced. Planar microcoils have been previously described for NMR experiments [24–28]. While the high-aspect ratio planar coil manufacturing technology can be successfully adopted for EPR microresonators, the NMR lumped tuning and matching circuits are difficult to transfer to a high-frequency range. To eliminate an increasing influence of parasitic capacitances and inductances as well as radiation issues, integrated elements have to be used. At microwave frequencies reduced dimensions of the distributed tuning/matching elements allow to design relatively simple and easily tunable microresonator layouts.

The cw EPR operation of a microcoil-based probe on micrometer-sized samples was recently demonstrated at 1.4 GHz (L band) [29]. At 300 K, a spin sensitivity of about 10^{10} spins $\cdot$ $G^{-1}Hz^{-1/2}$ was achieved, which is already comparable to that of a commercial X-band spectrometer. Sensitivity as high as 10^8 spins $\cdot$ $G^{-1}Hz^{-1/2}$ has been predicted for the 10 GHz version.

In this article, we demonstrate an operation of the planar microresonator (PMR) at 14 GHz, achieving a spin sensitivity of 2.3×10^9 spins $\cdot$ $G^{-1}Hz^{-1/2}$ at 300 K. The resonator has excellent power handling properties, generating 24 ns $\pi/2$ pulses with as little as 17 mW of microwave power.

2. Microresonator design and analysis

Our microresonator design uses a planar microcoil with integrated tuning elements. Planar structures are ideal to be manufactured by standard microtechnology. As open structure, they offer easy access to the sample space, for optical access, as well as for gradient and modulations fields. Planar geometries are also ideal for measurements on surface or monolayer samples. The substrate material used for the PMR should have low dielectric losses and high thermal conductivity. Low losses are important to improve the microresonator performance, whereas the high thermal conductivity substrate provides a heat sink for the power dissipated in the resonator elements. All above requirements are met by high resistivity silicon (>2500 Ωcm) [30,31]. As an alternative substrate, we used a ceramic-polymer composite with high dielectric constant (R6010LM from Rogers Corp.).

Our main optimisation criterion is the signal-to-noise ratio of the microresonator. The voltage ε induced by the precessing magnetisation $\mathbf{M}$ in the EPR coil can be calculated using the principle of reciprocity [32]

$$\varepsilon(t) = -\int_{V_s} \frac{\mathrm{d}}{\mathrm{d}t}(\mathbf{B_{1u}}(\mathbf{r})\mathbf{M}(t,\mathbf{r}))\,\mathrm{d}V_s, \tag{1}$$

where $\mathbf{B_{1u}}(\mathbf{r}) = \mathbf{B_{1u}}(\mathbf{r},t)/\mathrm{i}(t)$ is the magnetic field at position $\mathbf{r}$ produced by a unitary current carried by the microcoil and $\mathbf{M}(\mathbf{r},t)$ is the spin magnetisation at this position.

The magnitude of B_{1u} (in T/A) is proportional to the microwave efficiency factor Λ [20] (in $T/W^{1/2}$). The amplitude of a free induction decay signal produced by the sample, which has been subjected to a $\pi/2$ pulse ($M_{xy=}M_0$), is then given by [33]

$$\varepsilon_0 = \omega_0 B_{1u,xy} M_0 V_s. \tag{2}$$

Here ω_0 is the EPR resonance frequency, $B_{1u,xy}$ is the component of the average microwave field perpendicular to the static magnetic field, M_0 is the static equilibrium magnetisation

$$M_0 = \frac{ng^2\mu_B^2 S(S+1)B_0}{3kT}, \tag{3}$$

n is the number of spins at resonance per unit volume, g is the Landé factor, S is the electron spin, and T is the sample temperature, μ_B stands for the Bohr magneton. For small samples, the transverse magnetic field amplitude at the position of the sample can be used for $B_{1u,xy}$; for extended samples, it must be averaged over the sample.

To calculate the limiting noise, we consider the thermal noise from the active resistance R of the coil,

$$N_{RMS} = \sqrt{4kTR\Delta f}. \tag{4}$$

Here, T is the temperature of the coil and Δf is the bandwidth of detection electronics. Both signal and noise are transformed by the tuning/matching circuitry and amplified in the detection setup. Taking into account noise figures and gains of all components of the receiver, the noise of the whole spectrometer can be obtained from Friis formula [34]. Calculated signal-to-noise ratio can be compared to the measured one, allowing to optimise the performance of the PMR and the whole detection setup.

The signal from the microcoil can be maximised by increasing microwave efficiency factor of the microresonator. The noise can be reduced by minimising the resistance of the coil trace R. Thus, the signal-to-noise

ratio of the PMR can be optimised by adjusting the microcoil dimensions

$$(S/N) \propto B_{1u,xy}/\sqrt{R}. \quad (5)$$

For a given microwave power and sample dimensions, the magnetic field in the coil is maximised by reducing the dimensions of the coil. The trace width has to be scaled together with the coil radius to keep the optimal microwave efficiency factor. Λ scales inversely proportional to the radius of the planar coil as long as the coil trace width remains small compared to its radius; otherwise, the dependence becomes logarithmic. A thicker metallisation layer increases the active surface of the coil trace and thus reduces the influence of the skin effect at high frequencies and the active resistance of the coil. Magnetic susceptibility issues are not critical for our application, so electroplating by pure copper was used to produce the PMRs.

To achieve efficient microwave power transfer to the PMR coil and acquisition of the signal from the sample, the impedance of the PMR must be matched to the 50 Ω coaxial line. Tuning and matching of the coil improves also the signal-to-noise ratio of the receiver, because most preamplifiers have the noise figure optimised for 50 Ω input impedance. The microwave power from a commercially available coaxial connector (SMA) has to be coupled to the PMR through the planar line. The microstrip line design with passive coupling elements was chosen for the prototype. The elements of the layout were shaped using the relatively cheap and flexible "repro" lithography. With the available equipment, this process yielded elements with 50 μm feature size.

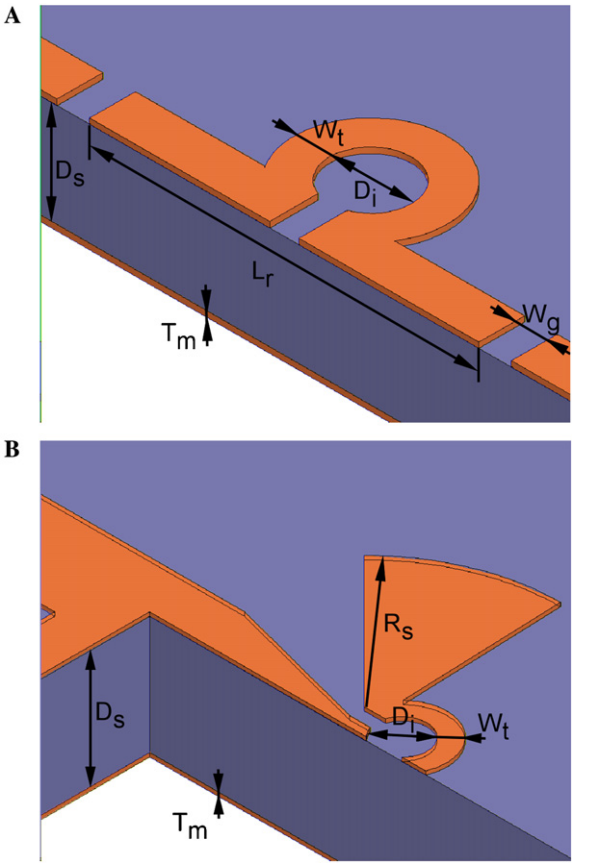

Fig. 1. Cross section of the microstrip resonator with an incorporated coil. (A) Layout on the 20 × 20 mm R6010LM substrate, coil diameter $D_i = 500$ μm, trace width $W_t = 220$ μm, resonator length $L_r = 2.39$ mm, gap width $W_g = 180$ μm, substrate thickness $D_s = 635$ μm, copper thickness $T_m = 35$ μm. (B) Layout on the high resistivity 12 × 12 mm Si substrate, coil diameter $D_i = 200$ μm, trace width $W_t = 80$ μm, radial stub radius $R_s = 790$ μm, radial stub angle 45°, rectangular stub length 2.1 mm, substrate thickness $D_s = 475$ μm, copper thickness $T_m = 15$ μm. The ground plane of both resonators is fully metallised. The microstrip-to-SMA connectors are not shown.

3. Simulation of resonators

Two different layouts were designed, implementing two different approaches for matching/tuning of the planar microcoil. In the first one, (Fig. 1A) a resonance in the microstrip line section was used to set the operation wavelength, whereas the gaps on both sides of the line served for adjustment of the resonance depth and quality factor. To make the design scalable, a single turn coil was incorporated into the microstrip resonator. This design was manufactured on R6010LM and Si substrates with coil diameters of 500 μm and 200 μm, respectively. The microwave signal is connected to the microresonator through an SMA-to-microstrip connector on one side; the other side is connected to ground through a 50 Ω coaxial load.

In the second type of the matching/tuning circuit, the radial stub was used for tuning the operation frequency, whereas the shunt stub of an appropriate length matched the microresonator to the microstrip line impedance (Fig. 1B). The microwave signal is fed to the PMR through an SMA-to-microstrip connector. Parasitic capacitances to the ground plane did not allow this type of resonator with the 500 μm coil on R6010LM substrate, so only the version with 200 μm coil on the Si substrate was manufactured.

Some of the design parameters were determined by the manufacturing process. Its resolution (minimal achievable gap width) limited the minimal coil diameter. The trace height of 35 μm on the laminated R6010LM substrate is determined by the thickness of the copper foil. On the Si substrate, we used electrodeposition to increase the trace thickness to 15 μm.

At the first stage of the design procedure, the initial dimensions of the planar microcoils were determined semi-analytically optimising their signal-to-noise ratio (Eq. (5)). The initial microstrip line section length for the first PMR design was then estimated for the simple microstrip resonator without an incorporated coil

$$(L_r + \Delta L_r) = \frac{c}{2f_0\sqrt{\varepsilon_{eff}}}, \quad (6)$$

where f_0 is the resonance frequency, ε_{eff} is the effective dielectric constant of the microstrip line and ΔL_r is the extra length contributed by microstrip gap. ε_{eff} and ΔL_r can be determined using existing analytical approximations [35], but we have found it more convenient to use the closed form model of the microstrip line from Ansoft Designer. The obtained microstrip line length L_r served then within a finite element method simulation software (HFSS, Ansoft) as an initial value for the optimisation procedure minimising the reflection coefficient of the PMR at f_0.

In the case of the PMR with the radial stub, the geometrical coil dimensions obtained from optimisation of Eq. (5) were inserted into the planar inductor model [36] to determine coil inductance and resistance. The lumped element model of the planar microcoil with those parameter values has been then adopted in Ansoft Designer together with closed form radial stub model as tuning element and the rectangular open stub model as matching element to calculate their dimensions required to tune and match the PMR at f_0. First the tuning stub dimensions were optimised to make the real part of the serial coil-stub circuit impedance equal to 50 Ω, then the second optimisation procedure was performed to find the length and position of the open stub that would cancel the imaginary part of the PMR impedance. The PMR model with those initial geometrical dimensions was then again optimised in HFSS. Simultaneous radial stub radius and rectangular stub length and position optimisation (three parameters procedure) resulted in the final design layout. For both designed layouts only the full electromagnetic simulation including the influence of all parasitic impedances, dispersion in the line, and radiation losses allowed for accurate determination of the tuning and matching elements dimensions.

The simulation of the microstrip resonator with the incorporated microcoil reveals the electric field concentration on the line ends (Fig. 2A), as expected for the microstrip resonator, and strong magnetic field (Fig. 2B) within the coil. Both field components are quite well spatially separated. The magnetic field distribution in the coil is quite nonuniform, following the $1/r$

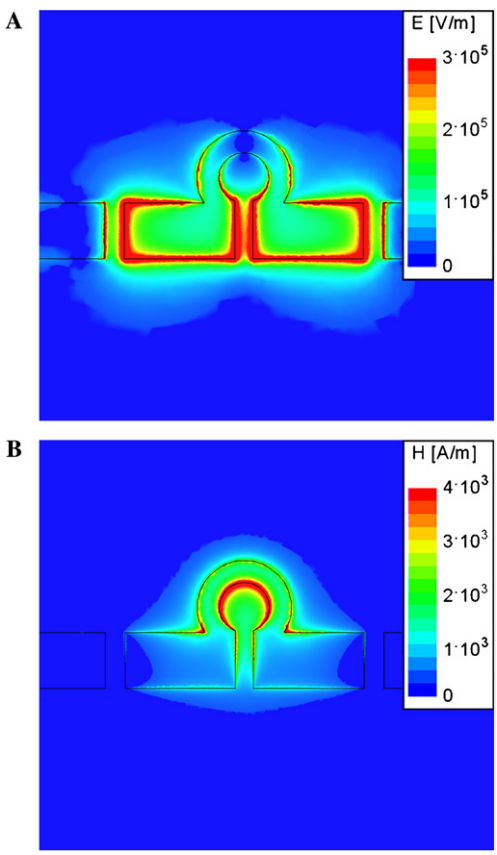

Fig. 2. Electric (A) and magnetic (B) field distribution in the microstrip resonator with an incorporated coil on the R6010LM substrate, coil diameter 500 μm.

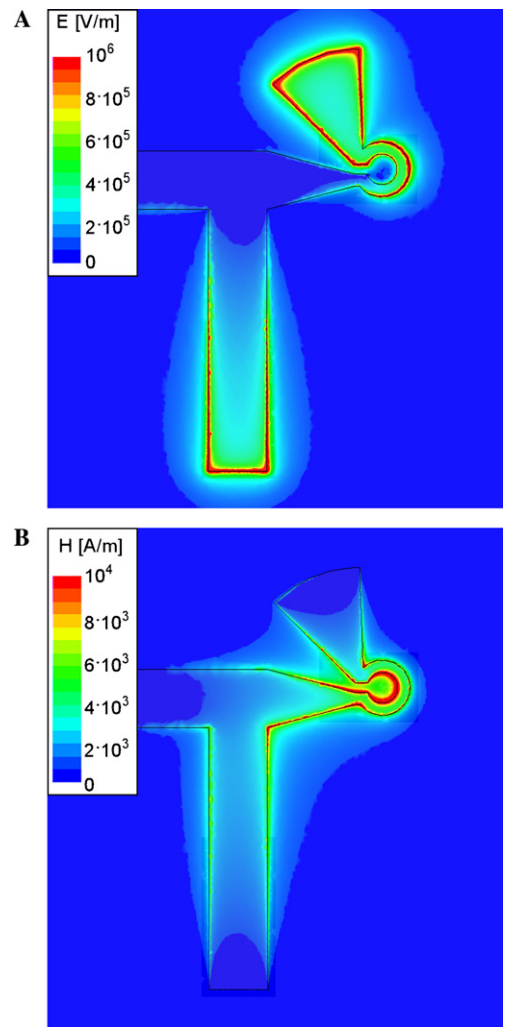

Fig. 3. Electric (A) and magnetic (B) field distribution in the microresonator on a high resistivity Si substrate, coil diameter 200 μm.

dependence, where r is the distance from the coil trace. The strongest field appears at the inner edges of the coil. The simulated scattering matrix data allow us to characterise the quality of the PMR. We define a depth of the resonance as a reflection coefficient at the resonance frequency and a loaded quality factor from the half-power resonance bandwidth Δf as $Q = f_0/\Delta f$. Δf was obtained from the Lorentzian fit of the power transmission coefficient for the microresonator with an incorporated microcoil and power reflection coefficient for the PMR with radial stub. Despite of a relatively low quality factor of the structure ($Q_{th} \approx 50$) and the resonance depth of 0.32 (−10 dB), the microwave efficiency factor in the coil centre reaches $\Lambda_{th} = 2\ \mathrm{mT/W^{1/2}}$. Scaling the coil down to 200 μm increases the efficiency factor inversely proportional to the diameter, up to 5.4 $\mathrm{mT/W^{1/2}}$. In the design with two stubs (Fig. 3) the electric field is also concentrated at the stub ends, while the magnetic field is concentrated within the coil. This microresonator has slightly higher quality factor ($Q_{th} \approx 70$) and deeper resonance 0.04 (−30 dB) but with the same coil diameter of 200 μm quite similar $\Lambda_{th} = 6.3\ \mathrm{mT/W^{1/2}}$. This means, that for the reasonably tuned PMR the latter is determined by the coil diameter.

For the realisation of the Si microresonators, we used thin film technology including an electroplating process.

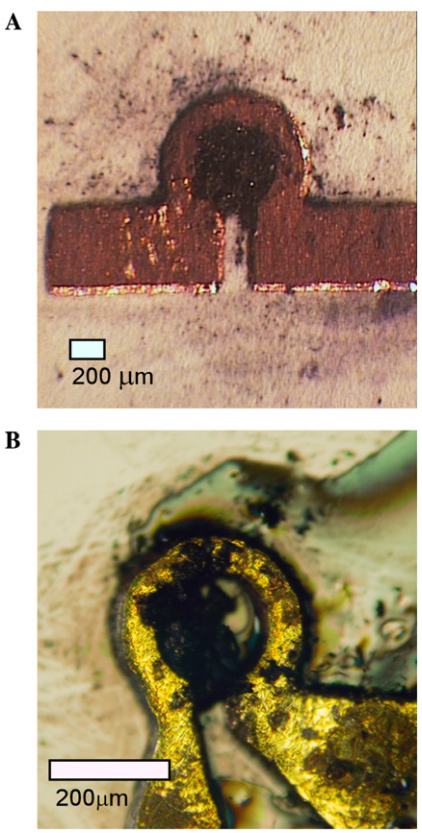

Fig. 4. Photos of the microresonators filled with DPPH: (A) PMR on R6010LM substrate, coil diameter 500 μm; (B) PMR on Si substrate, coil diameter 200 μm.

The optimised design obtained from the simulation was transformed into a lithographical mask. To optimise adhesion, a thin Ti layer was deposited on the Si wafer, and on this layer we sputtered a 300 nm copper seed layer. Electroplating deposited additional copper onto this seed layer, for a resulting thickness of 15 μm.

4. Microresonator performance

For the sensitivity tests PMRs were loaded with standard 2,2-diphenyl-1-picrylhydrazil (DPPH) samples (Fig. 4). The spin density of DPPH is about $n = 2 \times$

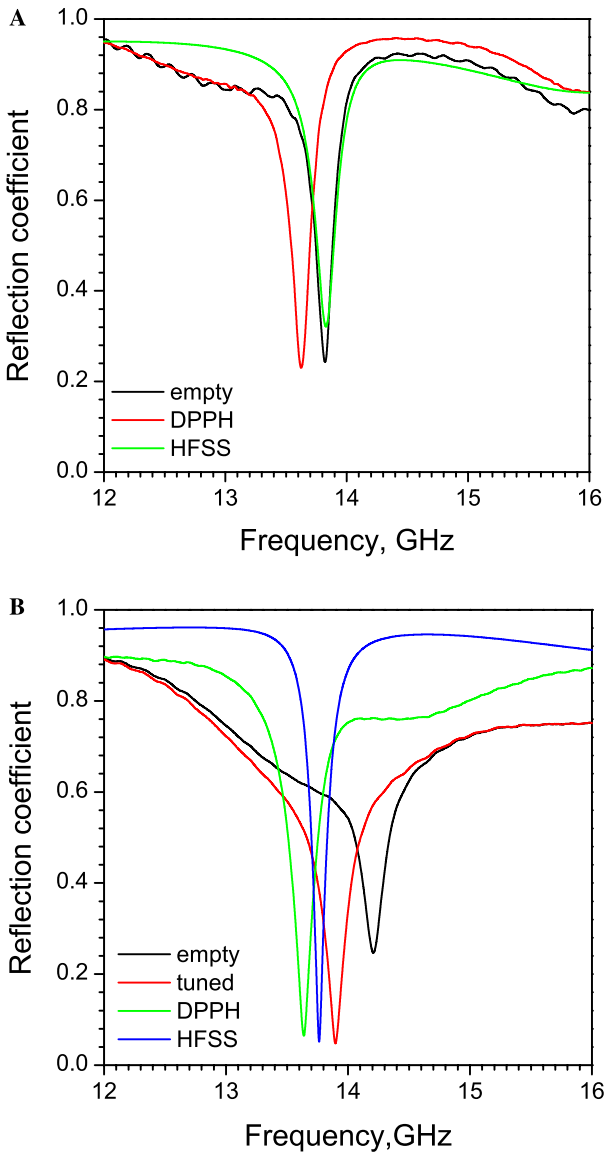

Fig. 5. Experimental and simulated reflection coefficients of the microresonators: (A) 500 μm PMR on R6010LM substrate (quality factor with a sample $Q_{exp} = 50$); (B) 200 μm PMR on Si substrate (quality factor with a sample $Q_{exp} = 37$). The curves marked as "DPPH" were acquired after the sample loading.

$10^{27}\,m^{-3}$. The sample volume V_s was estimated from the measurements made with the microscope, being about $(190\,\mu m)^3$ and $(78\,\mu m)^3$ in the microresonators on R6010LM substrate and on Si substrate respectively.

The matching and tuning quality of the PMRs was tested with a network analyser (Fig. 5). The impedance matching and tuning of the microresonators depends on the precision of the manufacturing. In the manufactured PMR on Si substrate, the thickness of the copper layer was larger than in the simulation (30 μm vs. 15 μm). Together with a smaller gap between the ends of the coil (52 μm vs. 60 μm), this shifted the resonance frequency by about 400 MHz, as we could verify by appropriate numerical modelling. In addition, the increased thickness of the metallisation layer introduced additional resonances. Both devices had lower Q values than predicted by the simulation. This can be attributed to the roughness of the copper metallisation and therefore increased radiation losses. The PMR with radial stub was tunable by up to 500 MHz by placing small (a few millimetre) pieces of dielectric material with high dielectric permittivity ($\varepsilon \sim 10$) in the high electric field concentration area over the radial stub. In our devices, no additional matching was required, but we assessed the possibility by placing another piece of the dielectric ($\varepsilon \sim 3$) above the rectangular stub of the PMR. This changed the imaginary part of the impedance by about 10 Ω; it also shifted the resonance frequency by about 100 MHz. Additional frequency shifts were caused by the sample placed in the coil and multiple reflections in the feedlines of the EPR setup. The obtained quality factor of the microresonators on R6010LM, even after the tuning procedure and sample loading, was still close to the theoretically predicted value $Q_{th} \approx 50$, whereas the microresonators on Si were more broadband than theoretically predicted, but with deeper resonance than the version on R6010LM.

5. CW EPR

EPR experiments with the PMRs have been performed using a 14GHz home-built spectrometer (Fig. 6). The components of the setup are listed in the figure caption.

Electron paramagnetic resonance with DPPH samples was measured in the microresonators on R6010LM and Si substrate (Fig. 7). The maximal CW EPR sensitivity was obtained with an input microwave power of 33 μW for the 500 μm PMR and 16 μW for the 200 μm PMR. The signal-to-noise ratios, S/N defined as peak-to-peak signal amplitude to the root-mean-square of the noise, were 6.8×10^5 for the microresonator on R6010LM and 3.5×10^5 for the one on Si. Measured S/N values were considerably lower than expected from the simulation. For the microstrip resonator with an incorporated microcoil the signal calculated using Eq. (2) of [29] exceeds the experimentally observed signal by a factor of 3, and for the PMR with the radial stub by a factor 1.5. The calculation was done assuming that the DPPH samples are far from saturation, whereas in the experiment they are partially saturated. The measured noise was twice as large as the calculated thermal noise generated by the series resistance of the microcoil. The additional noise is most

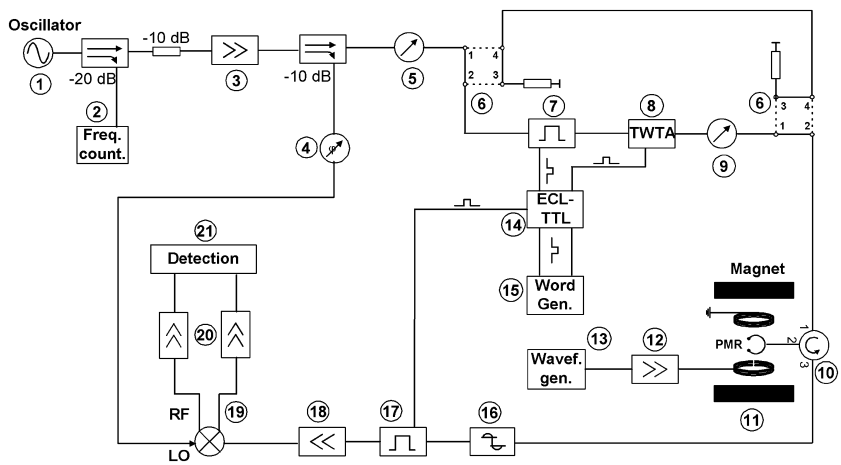

Fig. 6. Schematic of the EPR spectrometer used for the PMR testing. (1) 14 GHz oscillator (Miteq OTC-1CM-134-141-15P-AFC), (2) frequency counter (XL Microwave 3400 A), (3) 25 dB microwave amplifier (MA Ltd. AL7-13.4-14.1-25-30), (4) phase shifter (ARRA 9426B), (5) variable attenuator (Alan 50CA 14,8-2118), (6) transfer switches (Narda XSEM323LD), (7) pulse forming 2 ns rise/fall time PIN switch (Miteq 124796), (8) travelling wave tube amplifier (ASI Inc. 117Ku), (9) high power variable attenuator (ARRA 9684-60S), (10) circulator (Quest SR1015T01), (11) 1.4 T electromagnet (Bruker), (12) home-built audio-freq. amplifier, (13) waveform generator (Hameg HM 8130), (14) home-built ECL-TTL converter, (15) word generator (Interface Technology RS-690), (16) limiter (ACLM-4601C36K), (17) blanking switch (Miteq QN138BDF1), (18) 30 dB low noise microwave preamplifier (MA Ltd. AL22-13-15-30), (19) quadrature mixer (Anaren 250129), 30dB videoamplifiers (Miteq AU-1534), (21) detecion: for CW operation lock-in amplifiers (Stanford Research SR 830), for pulse operation scope (LeCroy WR6050), data acquisition on Macintosh computer using home-written MacExp software.

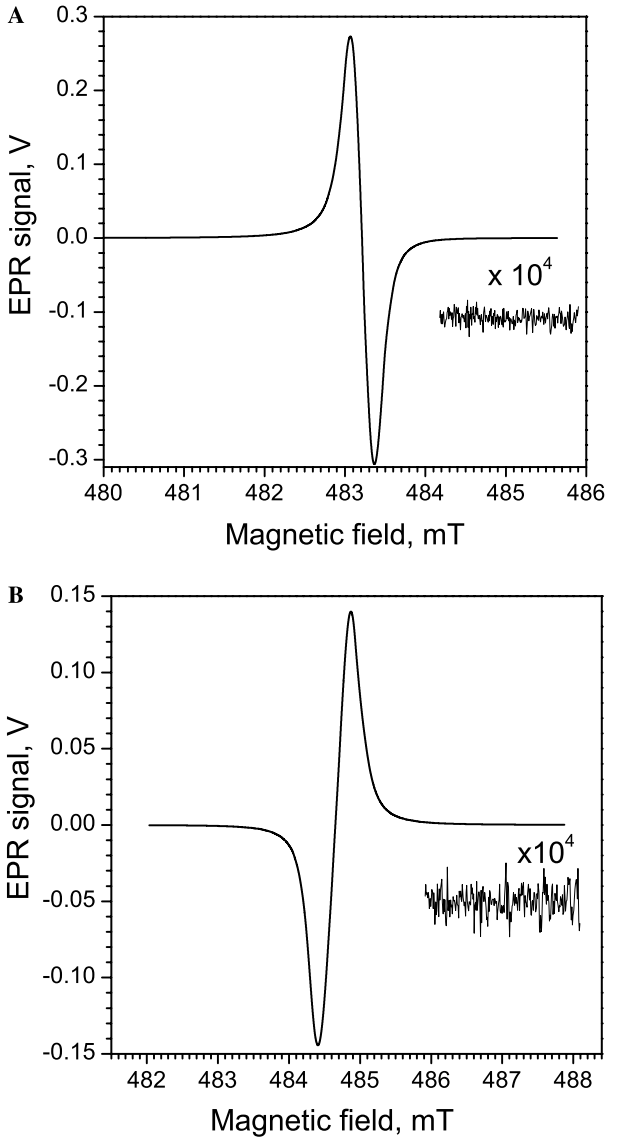

Fig. 7. EPR signals of the DPPH samples: (A) in the 500 μm PMR on R6010LM substrate, $f_0 = 13.55$ GHz, magnetic field modulation amplitude $B_m = 0.3$ mT, (B) in the 200 μm PMR on Si substrate, $f_0 = 13.59$ GHz, $B_m = 0.46$ mT. In both cases magnetic field modulation frequency was $f_m = 20$ kHz, lock-in time constant 300 ms and the filter slope 12 dB/octave, resulting in the equivalent noise bandwidth of 0.417 Hz.

likely due to phase noise of the microwave source, which was not taken into account in the calculation.

If we define the spin sensitivity as the minimum number of detectable spins for a frequency bandwidth f of 1 Hz [29]

$$N_{\min} = \frac{nV_s}{(S/N)\sqrt{f}}, \tag{7}$$

the sensitivity in spins/$\mathrm{Hz}^{1/2}$ is then 3.2×10^{10} and 4.3×10^9, respectively, for the two tested devices. Dividing by the linewidth of 1.9 G reported for DPPH [37], this corresponds to a sensitivity of 1.7×10^{10} and 2.3×10^9 spins $\cdot\, \mathrm{G}^{-1}\mathrm{Hz}^{-1/2}$.

In the CW EPR experiment with the DPPH samples, the measured sensitivity of the device scaled inversely proportional to the square of the microresonator diameter. The reduction of the diameter by a factor 2.5 increased the sensitivity by a factor of 7, somewhat more than what is expected from Eq. (5). Within the validity of the quasistatic approximation, we expect that the magnetic field drops off inversely proportional to the distance, $B_{1u,xy} \propto 1/d$, while the resistivity should increase with the diameter, $R \propto d$, where d is the coil diameter. For a constant number of spins in the coil, we therefore expect the sensitivity to increase as $(S/N) \propto d^{-3/2}$ The biggest uncertainty in this comparison is the estimation of the sample size, i.e., number of spins $N_s = nV_s$ which may be as large as ±30%.

6. Pulsed EPR

We evaluated the performance of the microresonators for pulsed experiments by applying (nominal) π/2 microwave pulses and measuring the free induction decay (FID) signals after the dead time of the spectrometer (up to 100 ns) (Fig. 8). The signal-to-noise ratio, defined as the ratio of the maximal FID signal to the rms noise, was calculated from these results (see Table 1). The calculated signal-to-noise ratios are in reasonable agreement with the experimentally measured values. Since the microwave field is rather inhomogeneous over the sample, it is not possible to uniformly excite all the spins in the sample, resulting in a somewhat smaller signal. In addition, the inhomogeneity has to be taken into account for the calculation of the expected signal size. The transverse relaxation time measured from the FID slope (T_2^*) was 40 ns, below the literature data for DPPH ($T_2 = 62$ ns).

The pulsed experiments provided a direct measurement of the microwave efficiency factor. The calculated microwave efficiency factors Λ_{cor}, corrected for the experimentally determined Q_{exp} of the microresonator $\Lambda_{cor} = \Lambda_{th}\sqrt{Q_{exp}/Q_{th}}$, are in reasonable agreement with experimentally determined values Λ_{exp} (Table 1). The optimal pulse power calculated at the fixed π/2-pulse length, using these efficiency factors, was 34.5 mW for the resonator on R6010LM, whereas the maximal FID signal value was obtained at 42.5 mW (Fig. 8A). The difference of approximately −1 dB corresponds quite well to the attenuation of the coaxial lines between the circulator and the probe head of the EPR spectrometer. For the 200 μm coil on Si substrate, the calculated optimal field was reached with a microwave power of 6.5 mW, whereas the maximum signal was obtained at 16.7 mW (Fig. 8B). The discrepancy is partly due to the inhomogeneous coil loading with the sample. Nevertheless the

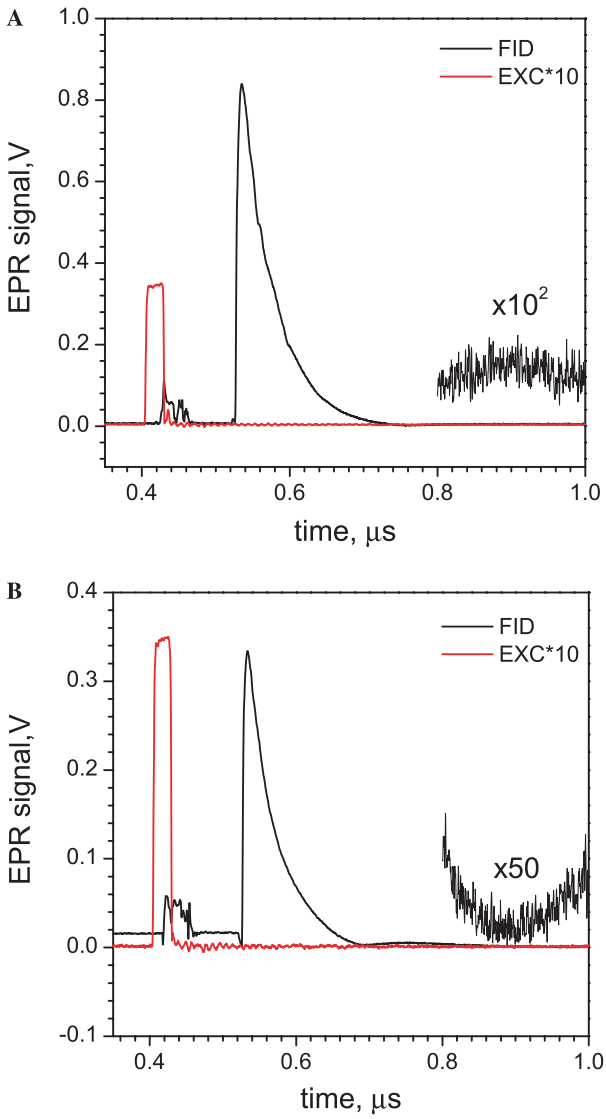

Fig. 8. Experimental FID's of DPPH samples measured in the microresonators using 24 ns π/2 excitation pulses: (A) 500 μm PMR on R6010LM substrate, pulse power 42.5 mW, (B) 200 μm PMR on Si substrate, pulse power 16.7 mW. Presented data were averaged over 1000 shots.

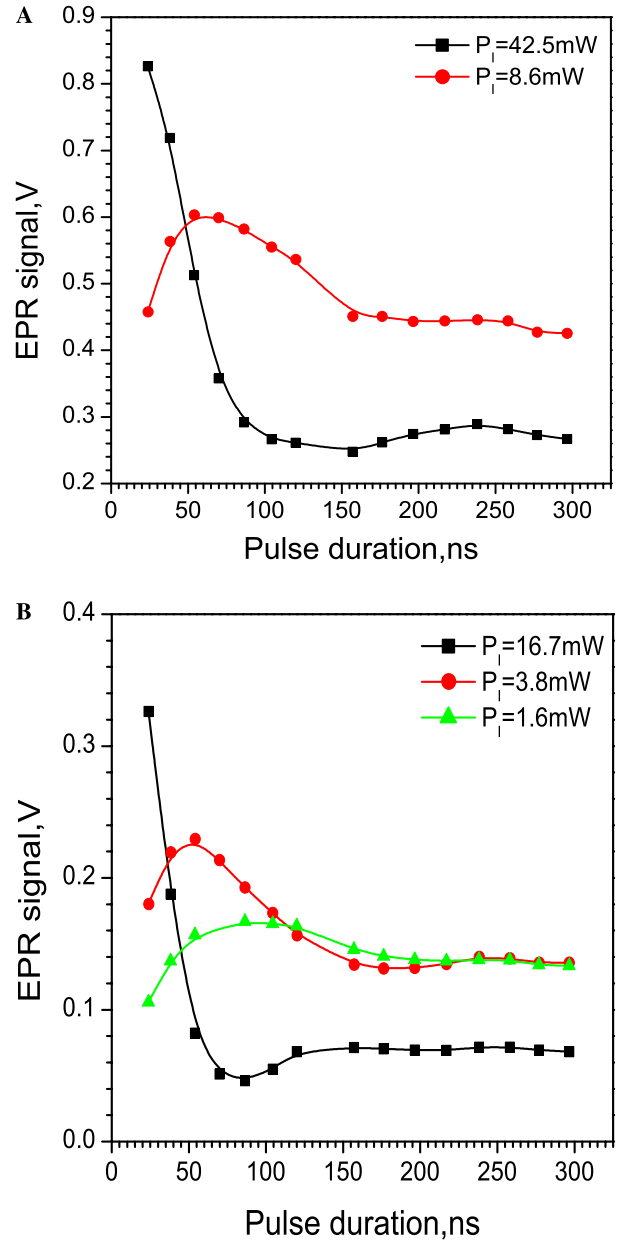

Fig. 9. Dependence of FID signal amplitude on the excitation pulse length and input power measured in the microresonators: (A) 500 μm PMR on R6010LM substrate, (B) 200 μm PMR on Si substrate.

power level required is here much lower than in the standard cavity. With this extremely low power level in the EPR experiments with the microresonators it is no longer necessary to use travelling wave tube amplifiers.

The FID amplitude dependence on the pulse duration characterises the $\mathbf{B_1}$ magnetic field distribution in the microresonators (Fig. 9). At any applied pulse length the FID signal remains positive. The magnetic field in the microresonator is not uniform enough over the sample to flip all the spins simultaneously. For EPR applications where the uniform microwave field strength is

Table 1
Calculated signal-to-noise ratios and microwave efficiency factors of the microresonators compared to experimental data measured by pulsed EPR

D_i, mm	N_s	S/N_{exp}	S/N_{th}	Λ_{exp}, mT/W$^{1/2}$	Λ_{cor}, mT/W$^{1/2}$	Λ_{th}, mT/W$^{1/2}$
0.5	1.4×10^{16}	1100	2340	1.8	2.0	2.0
0.2	9.4×10^{14}	560	557	2.9	4.6	6.3

required, the sample should not be located near to the inner coil edge.

7. Conclusions

We have realised two prototype microresonators for EPR experiments on small samples, using planar microcoil structures. The sensitivity of these microresonators is close to the theoretical limits. Low temperature operation should further increase the sensitivity by several orders of magnitude. The small volume of the microresonator results in excellent microwave efficiency: strong microwave fields can be generated with very little microwave power and therefore low power dissipation. The reduced power dissipation should be important for low temperature EPR experiments. We also expect that these microresonators will be useful in spin-based quantum information processors [38,39], where the "sample" may be as small as a few ($\sim$10–1000) spins.

The presented layouts have been designed at 14 GHz, but using the described simulation procedure similar circuits could be built for other EPR frequencies, e.g., X-Band (9.5 GHz). The current layout of the microresonator should be scalable down to tens of micrometers. This would result in a spin sensitivity of about 10^6 spins $\cdot$ $G^{-1}Hz^{-1/2}$ [29]. Recent achievements in the photonic crystals development demonstrated the possibility to operate split rings, nanometer sized planar LC resonators at THz frequencies [40]. However, reducing the device down to nanometer size would require a different electromagnetic wave coupling approach.

Other issues are the on-chip integration of the microresonator with the active elements in order to create micron-sized EPR spectrometer. Such devices were already proposed for NMR [41]. At high frequencies typical for EPR this would be a challenging engineering problem, but it can be solved on the basis of existing Si microtechnology.

Acknowledgment

This work was supported by the Information Societies Technology programme of the European Union under contract no. IST-2001-37150 (QIPDDF-ROSES project).

References

[1] K. Ohno, T. Mukami, Microscopic ESR imaging using a microcoil system, J. Magn. Reson. 79 (1988) 343–347.
[2] W.J. Wallace, R.H. Silsbee, Microstrip resonators for electron-spin resonance, Rev. Sci. Instrum. 62 (1991) 1754–1766.
[3] Sheng-Chiang Lee, C.P. Vlahacos, B.J. Feenstra, A. Schwartz, D.E. Steinhauer, F.C. Wellstood, S.M. Anlage, Magnetic permeability imaging of metals with a scanning near-field microwave microscope, Appl. Phys. Lett. 77 (2000) 4404–4406.
[4] F. Sakran, A. Copty, M. Golosovsky, N. Bontemps, D. Davidov, A. Frenkel, Electron spin resonance microscopic surface imaging using a microwave scanning probe, Appl. Phys. Lett. 82 (2003) 1479–1481.
[5] J.A. Weil, J.R. Bolton, J.E. Wertz, Electron Paramagnetic Resonance, Wiley, New York, 1994.
[6] D. Rugar, C.S. Yannoni, J.A. Sidles, Mechanical detection of magnetic resonance, Nature 360 (1992) 563–566.
[7] D. Rugar, R. Budakian, H.J. Mamin, B.W. Chui, Single spin detection by magnetic resonance force microscopy, Nature 430 (2004) 329–332.
[8] Y. Manassen, R.J. Hamers, J.E. Demuth, A.J. Castellano Jr., Direct observation of the precession of individual paramagnetic spins on oxidized silicon surfaces, Phys. Rev. Lett. 62 (1989) 2531–2534.
[9] C. Durkan, M.E. Welland, Electronic spin detection in molecules using scanning-tunnelingmicroscopy-assisted electron-spin resonance, Appl. Phys. Lett. 80 (2002) 458–460.
[10] J. Köhler, J.A.J.M. Disselhorst, M.C.J.M. Donckers, E.J.J. Groenen, J. Schmidt, W.E. Moerner, Magnetic resonance detection of a single molecular spin, Nature 363 (1993) 242–243.
[11] J. Wrachtrup, C.v. Borczyskowski, J. Bernard, M. Orrit, R. Brown, Optical detection of magnetic resonance in a single molecule, Nature 363 (1993) 244–245.
[12] A. Sienkiewicz, K. Qu, Ch.P. Scholes, Dielectric resonator-based stopped flow electron paramagnetic resonance, Rev. Sci. Instrum. 65 (1994) 68–74.
[13] M. Jaworski, A. Sienkiewicz, Ch.P. Scholes, Double-stacked dielectric resonator for sensitive EPR measurements, J. Magn. Reson. 124 (1997) 87–96.
[14] Y.E. Nesmelov, J.T. Surek, D.D. Thomas, Enhanced EPR sensitivity from a ferroelectric cavity insert, J. Magn. Reson. 153 (2001) 7–14.
[15] J.L. Davis, W.B. Mims, Endor cavity for electron spin echo experiments, Rev. Sci. Instrum. 49 (1978) 1095–1586.
[16] B. Johansson, S. Haraldson, L. Petterson, O. Beckman, A stripline resonator for ESR, Rev. Sci. Instrum. 45 (1974) 1445–1447.
[17] Ch.P. Lin, M.K. Bowman, J.R. Norris, A folded half-wave resonator for ESR spectroscopy, J. Magn. Reson. 65 (1985) 369–374.
[18] N.I. Avdievich, G.J. Gerfen, Multifrequency probe for pulsed EPR and ENDOR specroscopy, J. Magn. Reson. 153 (2001) 178–185.
[19] W. Froncisz, J.S. Hyde, The loop-gap resonator: a new microwave lumped circuit ESR sample structure, J. Magn. Reson. 47 (1982) 515–521.
[20] J.S. Hyde, W. Froncisz, T. Oles, Multipurpose loop-gap resonator, J. Magn. Reson. 82 (1989) 223–230.
[21] R.D. Britt, M.P. Klein, A versatile loop-gap resonator probe for low temperature electron spin-echo studies, J. Magn. Reson. 74 (1987) 535–540.
[22] S. Pfenniger, J. Forrer, A. Schweiger, Bridged loop-gap resonator: a resonant structure for pulsed ESR transparent to high-frequency radiation, Rev. Sci. Instrum. 59 (1988) 752–760.
[23] H. Mahdjour, W.G. Clark, K. Barbeschke, High sensitivity microwave spectroscopy with small nonresonant coils, Rev. Sci. Instrum. 57 (1986) 1100–1106.
[24] A. Webb, Radiofrequency microcoils in magnetic resonance, Prog. NMR Spectrosc. 31 (1997) 1–42.
[25] C. Massin, G. Boero, F. Vincent, J. Abenhaim, M. Bouterfas, P.-A. Besse, R.S. Popovic, High-Q factor RF planar microcoils for micro-scale NMR spectroscopy, Sensors and Actuators A 97 (2002) 280–288.
[26] L. Renaud, M. Armenean, L. Berry, P. Kleimann, P. Morin, M. Pitaval, J. O'Brien, M. Brunet, H. Saint-Jalmes, Implantable

planar rf microcoils for NMR microspectroscopy, Sensors and Actuators A 99 (2002) 244–248.
[27] S. Eroglu, B. Gimi, B. Roman, G. Friedman, R.L. Magin, NMR spiral surface microcoils: design, fabrication, and imaging, Concepts Magn. Reson. B 17B (2003) 1–10.
[28] C. Massin, F. Vincent, A. Homsy, K. Ehrmann, G. Boero, P.-A. Besse, A. Daridon, E. Verpoorte, N.F. de Rooij, R.S. Popovic, Planar microcoil-based microfluidic NMR probes 164 (2003) 242–255
[29] G. Boero, M. Bouterfas, C. Massin, F. Vincent, P.-A. Besse, R.S. Popovic, A. Schweiger, Electron-spin resonance probe based on a 100 μm planar microcoil, Rev. Sci. Instrum. 74 (2003) 4794–4798.
[30] J. Buechler, E. Kasper, P. Russer, K.M. Strohm, Silicon high-resistivity-substrate millimeter-wave technology, IEEE Trans. Microwave Theory Tech. 34 (1986) 1516–1520.
[31] A. Reyes, S.M. El-Ghazaly, S.I. Dorn, M. Dydyk, D.K. Schroeder, H. Patterson, Coplanar waveguides and microwave inductors on silicon substrates, IEEE Trans. Microwave Theory Tech. 43 (1995) 2016–2021.
[32] D.I. Hoult, The NMR receiver: a description and analysis of design, Prog. NMR Spectrosc. 12 (1978) 41–77.
[33] D.I. Hoult, R.E. Richards, The signal-to-noise ratio of the NMR experiment, J. Magn. Reson. 24 (1976) 71–85.
[34] A. vander Ziel, Noise, Sources, Characterization, Measurement, Prentice-Hall, 1970
[35] K.C. Gupta, R. Garg, R. Chandha, Computer Aided Design of Microwave Circuits, Artech House, 1981
[36] E. Pettenpaul, H. Kapusta, A. Weisgerber, H. Mampe, J. Lugisland, I. Wolff, CAD models of lumped elements on GaAs up to 18 GHz, IEEE Trans. on MTT 36 (1988) 294–304.
[37] S. Alger, Electron Paramagnetic resonance: Techniques and Applications, Wiley-Interscience, 1968
[38] M.A. Nielsen, I.L. Chuang, Quantum Computation and Quantum Information, Cambridge University Press, Cambridge, 2001.
[39] J. Stolze, D. Suter, Quantum Computing: A Short Course from Theory to Experiment, Wiley-VCH, Berlin, 2004.
[40] S. Linden, Ch. Enkirch, M. Wegener, J. Zhou, T. Koschny, C.M. Soukoulis, Magnetic response of metamaterials at 100 THz, Science 306 (2004) 1351–1353.
[41] G. Boero, J. Frounchi, B. Furrer, P.-A. Besse, R.S. Popovic, Fully integrated probe for proton nuclear magnetic resonance magnetometry, Rev. Sci. Instrum. 72 (2001) 2764–2768.